

## INCLINATION-INDEPENDENT GALAXY CLASSIFICATION

JEREMY BAILIN<sup>1</sup> WILLIAM E. HARRIS

Department of Physics & Astronomy, McMaster University, 1280 Main Street West, Hamilton, ON, L8S 4M1, Canada  
*Accepted for publication in ApJ.*

### ABSTRACT

We present a new method to classify galaxies from large surveys like the Sloan Digital Sky Survey using inclination-corrected concentration, inclination-corrected location on the color-magnitude diagram, and apparent axis ratio. Explicitly accounting for inclination tightens the distribution of each of these parameters and enables simple boundaries to be drawn that delineate three different galaxy populations: Early-type galaxies, which are red, highly concentrated, and round; Late-type galaxies, which are blue, have low concentrations, and are disk dominated; and Intermediate-type galaxies, which are red, have intermediate concentrations, and have disks. We have validated our method by comparing to visual classifications of high-quality imaging data from the Millennium Galaxy Catalogue. The inclination correction is crucial to unveiling the previously unrecognized Intermediate class. Intermediate-type galaxies, roughly corresponding to lenticulars and early spirals, lie on the red sequence. The red sequence is therefore composed of two distinct morphological types, suggesting that there are two distinct mechanisms for transiting to the red sequence. We propose that Intermediate-type galaxies are those that have lost their cold gas via strangulation, while Early-type galaxies are those that have experienced a major merger that either consumed their cold gas, or whose merger progenitors were already devoid of cold gas (the “dry merger” scenario).

*Subject headings:* galaxies: fundamental parameters — galaxies: structure

### 1. INTRODUCTION

Galaxies do not smoothly occupy the full range of possible structural and photometric parameter space. This fact was first pointed out by Hubble (1926), whose “Tuning Fork” classified galaxies into ellipticals, spirals, and barred spirals. The basic categorization of “early”-type galaxies, with a smooth quiescent elliptical appearance, and “late”-type galaxies, characterized by a spiral disk with sites of active star formation, has remained to this day.

Many studies have attempted to put this classification on a quantitative footing. Bimodality in the color-magnitude plane has been well established (e.g. Strateva et al. 2001; Blanton et al. 2003b; Baldry et al. 2004; Balogh et al. 2004), and provides the most straightforward classification method. Weinmann et al. (2006) classified galaxies into three types based on their colors and spectra: early-types, which are red and passive; late-types, which are blue and active; and intermediate-types, which are red and active. These authors argue that their intermediate class are most likely a combination of early-types whose star formation rates are overestimated and reddened edge-on late-types. Ellis et al. (2005) statistically studied the multivariate distribution of a large number of observed galaxy properties and found that exactly two classes are required. One particularly useful diagnostic plane for classifying galaxies is color versus global concentration of the light profile, where early-type galaxies appear red and concentrated while late-type galaxies appear blue and have low concentrations (e.g. Driver et al. 2006).

The use of such automated classifications is crucial in large galaxy surveys such as those now available, for

which visual examination of hundreds of thousands of galaxies is unfeasible<sup>2</sup>. Moreover, automated methods are important even when visual classifications are available, as they are quantitative and allow finer and unbiased classification in cases where the patterns identified by eye do not map correctly onto the physically-important parameters.

Most observational parameters that are used in classification methods are either calculated within a circular aperture or in circular annuli. However, disk galaxies are not usually circular when viewed on the sky, and their appearance varies systematically as a function of inclination. For example, the front and back sides of a disk contribute most of their light at small radii if the disk is highly inclined, but at large radii if the disk is nearly face-on; inclined disks therefore appear to be more concentrated. Observed colors and magnitudes are also affected by the increased dust absorption in highly inclined disks relative to nearly face-on disks. Inclination effects therefore introduce significant scatter in the observed parameters of individual disk galaxies.

Fortunately, it is possible to calculate and correct for the effects of inclination on several observed parameters. In Bailin & Harris (2008) (Paper I), a simple inclination-independent measure of galaxy concentration was derived based on the observed Petrosian concentration index  $C_{\text{Petro}}$  and the observed isophotal axis ratio  $b/a$  (see also Yamauchi et al. 2005, who recalculated the concentration in elliptical apertures directly from the galaxy images). Recently, four studies have used large samples of galaxies to determine the effects of inclination on galaxy photometry: Shao et al. (2007) (hereafter S07), Unterborn & Ryden (2008) and Maller et al. (2008), all using the Sloan Digital Sky Sur-

<sup>1</sup> bailinj@mcmaster.ca

<sup>2</sup> See, however, the Galaxy Zoo project: <http://galaxyzoo.org/>.

vey (SDSS), and Driver et al. (2007), using the Millennium Galaxy Catalogue (MGC), measured how the characteristic turnover in the luminosity function of spiral galaxies varies as a function of inclination, and provide simple parametrizations of the relative extinction in a galaxy as a function of disk inclination. These new methods allow us to correct galaxy properties for inclination effects and revisit the problem of automated galaxy classification.

In this paper, we present a new method for classifying galaxies that uses inclination-corrected values for galactic concentration, color, and absolute magnitude, along with the apparent axis ratio. We use the statistical power of SDSS, which allows us to examine the multivariate distribution of galaxy properties with ample signal-to-noise, and the MGC, which provides deep high-resolution images for direct visual classification. We describe the selection of the galaxy samples in section 2. The expressions for the inclination-corrected quantities are defined in section 3 and a face-on color-magnitude diagram of SDSS galaxies is presented. In section 4 we present our method of classifying galaxies and demonstrate its effectiveness, and finally we present our conclusions in section 5.

## 2. GALAXY SAMPLES

Our primary galaxy sample comes from SDSS, a 5-band optical and near-infrared imaging and spectroscopic survey covering one quarter of the sky (York et al. 2000). The final data release, DR6 (Adelman-McCarthy et al. 2007), contains imaging and spectroscopy of over half a million galaxies with well defined selection criteria. Our sample consists of the 486305 galaxies that meet the Main Galaxy Sample targeting criteria (Strauss et al. 2002), have spectra that are classified as galaxies with confident redshifts ( $z_{\text{conf}} > 0.85$ ), have dereddened Petrosian  $r$ -band magnitudes  $r < 17.7$ , lie in the redshift range  $0.01 < z < 0.2$ , and have absolute magnitudes  $M_r < -17.5$ . Petrosian magnitudes are used throughout, and  $r$ -band quantities are used for all photometric parameters. Colors and absolute magnitudes are  $k$ -corrected to  $z = 0$  with KCORRECT v4.1.4 (Blanton et al. 2003a). We adopt  $\Omega_0 = 0.3$ ,  $\Omega_\Lambda = 0.7$ , and  $H_0 = 70 \text{ km s}^{-1} \text{ Mpc}^{-1}$ .

While SDSS provides us with the statistics necessary to measure the multivariate distribution of galactic parameters, the imaging is relatively shallow and often taken in poor seeing conditions. Therefore, in order to obtain confident visual classifications of a subset of galaxies, we have used the deeper and higher resolution imaging data from the MGC (Liske et al. 2003). This  $37.5 \text{ deg}^2$   $B$ -band survey is entirely contained within the SDSS footprint, allowing cross-identification of all galaxies. We have randomly selected 400 SDSS galaxies from the above sample that are also contained in the cleaned bright MGC galaxy catalog<sup>3</sup> for direct visual classification.

## 3. CORRECTING FOR INCLINATION

### 3.1. Concentration

<sup>3</sup> Note that the default matched `mgc_sdss` catalog contains objects that lie in MGC exclusion regions and are therefore not suitable for scientific analysis. We have obtained a version of the `mgc_sdss` catalog cleaned of such objects from J. Liske.

In Paper I, we presented a method to correct the Petrosian concentration  $C_{\text{Petro}}$  for inclination effects. We briefly review the method here.

As disk galaxies are seen closer to edge-on, the isophotal axis ratio  $b/a$  decreases while the global concentration of the light profile increases. As a result, the loci of intrinsically similar galaxies in the  $C_{\text{Petro}}-b/a$  plane curve to higher  $C_{\text{Petro}}$  at smaller  $b/a$ . By constructing models of a pure exponential disk viewed at a variety of inclinations, we have determined the expected concentration of the disk  $C_{\text{Petro}}^{\text{disk}}$  as a function of the observed isophotal axis ratio  $b/a$ . We use this relationship to define the normalized concentration,  $C_{\text{norm},i}$ , for a galaxy with observed isophotal axis ratio  $(b/a)_i$  and observed Petrosian concentration  $C_{\text{Petro},i}$  to be:

$$C_{\text{norm},i} \equiv \frac{C_{\text{Petro},i}}{C_{\text{Petro}}^{\text{disk}}(b/a_i)}. \quad (1)$$

The loci of galaxies in the inclination-corrected  $C_{\text{norm}}-b/a$  plane no longer depend on axis ratio, validating the use of  $C_{\text{norm}}$  as an inclination-independent measure of galaxy concentration.

Note that although elliptical galaxies do not suffer from the same inclination effect as disks, they all have large apparent axis ratios. At these large axis ratios,  $C_{\text{Petro}}^{\text{disk}}$  is almost independent of  $b/a$ , and therefore the magnitude of the inclination correction is minimal. Therefore, applying the correction to all galaxies does not introduce any bias in the concentrations of elliptical galaxies.

### 3.2. Magnitudes and colors

S07 find that the extinction in an inclined disk galaxy relative to a face-on disk galaxy in a given band is well described by:

$$M - M^{\text{F}} = -\gamma_2 \log(\cos i) \quad (2)$$

for observed absolute magnitude  $M$ , face-on absolute magnitude  $M^{\text{F}}$ , inclination  $i$  (defined to be  $0^\circ$  for face-on disks and  $90^\circ$  for edge-on disks), and relative extinction coefficient  $\gamma_2$ . Values of  $\gamma_2$  for each SDSS band are given in S07.

In S07, the inclination  $i$  was determined from the apparent axis ratio of the exponential component of the surface brightness decomposition (“expab” in the SDSS database) by Monte Carlo simulations. We simply use the median mapping between expab and  $\cos i$  given in their figure 3. We then calculate the face-on absolute  $r$ -band magnitude,  $M_r^{\text{F}}$ , and face-on  $(g-r)$  color,  $(g-r)^{\text{F}}$ , using equation (2):

$$M_r^{\text{F}} = M_r + \gamma_2^r \log(\cos i) \quad (3)$$

$$(g-r)^{\text{F}} = (g-r) + (\gamma_2^g - \gamma_2^r) \log(\cos i). \quad (4)$$

Correcting for the disk inclination presumes the presence of a disk, while many galaxies are almost entirely spheroidal systems. Unlike the concentration (§ 3.1), the photometry is sensitive to the inclination correction even at relatively large axis ratios, and should be omitted for elliptical galaxies. We therefore only apply the correction to galaxies for which the bulge+disk surface brightness decomposition in SDSS contains at least a 20% disk, i.e. for which `fracdeV` < 0.8. We include

galaxies where the bulge contributes a large fraction of the flux (e.g. compared to S07, who restrict their analysis to  $\text{fracdeV} < 0.5$ , and Unterborn & Ryden 2008, who restrict their analysis to  $\text{fracdeV} < 0.1$ ) because the centrally-concentrated bulge light is severely attenuated by disk dust even in the absence of dust within the bulge itself, and therefore the inclination correction is vitally important even in systems with large bulges (Driver et al. 2007).

We plot the observed color-magnitude diagram (CMD) and the inclination-corrected face-on color-magnitude diagram in Figure 1. The marginal distributions of  $(g-r)$  and  $(g-r)^F$  are added as histograms. The basic bimodality of the CMD is apparent in both plots, with a red sequence and a blue cloud. In the observed CMD (left panel), the blue cloud appears to run into the red sequence at the luminous end and it is difficult to distinguish red from blue galaxies in this region. In contrast, the populations are much more clearly separated in the face-on CMD (right panel). Similarly, while the marginalized distribution of  $(g-r)$  contains a red peak with a blue tail, the marginalized distribution of  $(g-r)^F$  contains a distinct blue peak (see also Maller et al. 2008, who noted the increased separation between red and blue galaxies; and Unterborn & Ryden 2008, who noted the tightening of the blue sequence among galaxies with exponential profiles).

The effect of the inclination correction is directly demonstrated by the vector in the right panel, which indicates the inclination correction for a galaxy with  $i = 60^\circ$ . All inclination corrections occur parallel to this vector. The inclination correction moves galaxies almost perpendicular to the red sequence, which is why it makes a relatively large difference in the appearance of the CMD.

We have fit the red sequence by eye as

$$(g-r)^{\text{red}} = 0.77 + 0.02(M_r + 22). \quad (5)$$

This is indicated by the solid line in both panels of Figure 1. We define the location of galaxy  $k$  on the CMD relative to the red sequence as its CMD location parameter<sup>4</sup>:

$$\text{CMD}_k = (g-r)_k - (g-r)^{\text{red}}(M_{r,k}) \quad (6)$$

and analogously for the face-on CMD location parameter  $\text{CMD}^F_k$ :

$$\text{CMD}^F_k = (g-r)^F_k - (g-r)^{\text{red}}(M_{r,k}^F). \quad (7)$$

#### 4. INCLINATION-INDEPENDENT CLASSIFICATION

Traditionally, galaxies have been classified into two types: “early-type” or “elliptical” galaxies, which are red, round, smooth, and have centrally-concentrated light profiles well approximated by the de Vaucouleurs (1948)  $R^{1/4}$  law or the Sérsic (1968) profile with large values of  $n$ ; and “late-type” or “spiral” galaxies, which are blue, disk-shaped, contain spiral and clumpy structure, and have less concentrated exponential light profiles or Sérsic profiles with low values of  $n$ . An intermediate “lenticular” or “S0” classification is also sometimes used,

<sup>4</sup> Note that these definitions differ somewhat from the CMD location parameter used in Paper I.

TABLE 1  
COMPARISON BETWEEN VISUAL AND AUTOMATED CLASSIFICATIONS

Visual Classification	Total	Automated Classification		
		Early	Intermediate	Late
E	133	72	49	12
E/L	36	15	15	6
S/L	45	8	17	20
S	174	8	13	153
X	12	6	3	3
Total	400	109	97	194

although it is often considered an extension of either the elliptical or spiral class depending on context.

In this section, we attempt to put these classifications on a firm quantitative footing by using the inclination corrections developed in section 3 to define an inclination-independent method of classifying galaxies.

##### 4.1. Visual classification

We have randomly selected 400 galaxies contained in both our SDSS sample and the MGC and inspected the MGC images by eye. The advantages of the MGC images are several: (1) they are deeper than the SDSS images, allowing us to see fainter features in the outer regions of the galaxy that can aid in classification, (2) the typical seeing in the MGC is better than in SDSS, allowing effectively higher resolution, and (3) by using single-band images we explicitly ensure that our visual classification is purely based on the morphology and has no color bias.

Each galaxy was given one of 5 classifications: “elliptical” (E), “elliptical/lenticular” (E/L), “spiral/lenticular” (S/L), “spiral” (S), or “unclassifiable” (X; usually a major merger). Table 1 lists the number of galaxies given each classification.

##### 4.2. Automated classification

Our primary classification is performed in the color-concentration plane (e.g. Driver et al. 2006). We adopt the CMD location parameter as the measure of color, as it provides a better estimate of whether a galaxy lies on or off the red sequence than  $(g-r)$  alone. The joint distribution of observed concentrations  $C_{\text{Pet}ro}$  and observed CMD locations is shown in the left panel of Figure 2, along with the distribution of each parameter independently. The tendency for red galaxies to be more concentrated is apparent, as is an overall bimodality of the galaxy population: there is a strong peak of red galaxies at high concentrations ( $2.5 \lesssim C_{\text{Pet}ro} \lesssim 3.4$ ) and a more spread-out tail of blue galaxies at low concentrations.

The right panel of Figure 2 shows the joint and individual distributions of the inclination-corrected concentration  $C_{\text{norm}}$  and the face-on color  $\text{CMD}^F$ . The inclination correction makes several appreciable improvements to this diagnostic plane. Firstly, as described in Paper I, the distribution of  $C_{\text{norm}}$  is *trimodal*: there is a distinct grouping of galaxies at intermediate concentrations. This trimodality has been previously unrecognized because inclination effects smear together the intermediate- and high-concentration subpopulations. The color distributions, and therefore the luminosity-weighted stellar age, of these two populations are similar, but they have distinct morphologies. Secondly, the distribution of  $\text{CMD}^F$

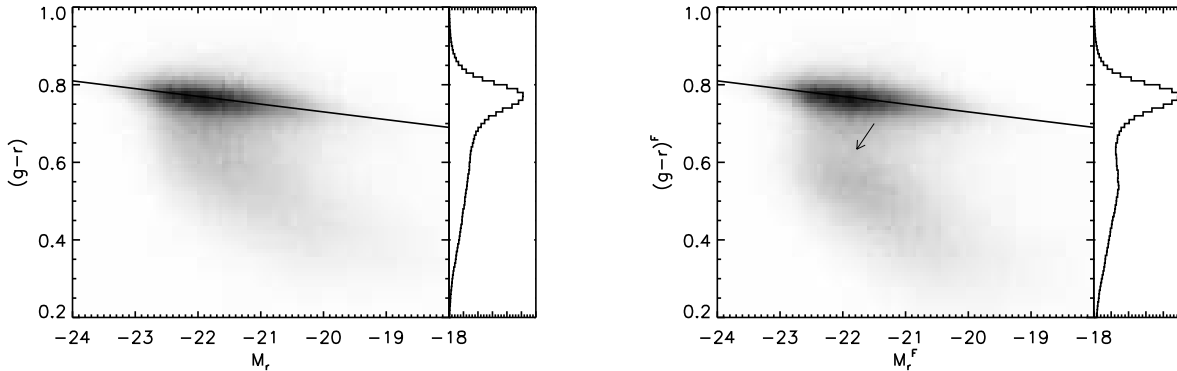


FIG. 1.— (*Left*) Observed rest-frame  $(g-r)$  color versus  $M_r$  color-magnitude diagram for SDSS galaxies. The distribution of  $(g-r)$  marginalized over absolute magnitude is shown in the histogram on the right. The solid line denotes the red sequence. (*Right*) As in the left panel, but for face-on color  $(g-r)^F$  versus face-on absolute magnitude  $M_r^F$ . The vector denotes the inclination correction for a galaxy with  $i = 60^\circ$ .

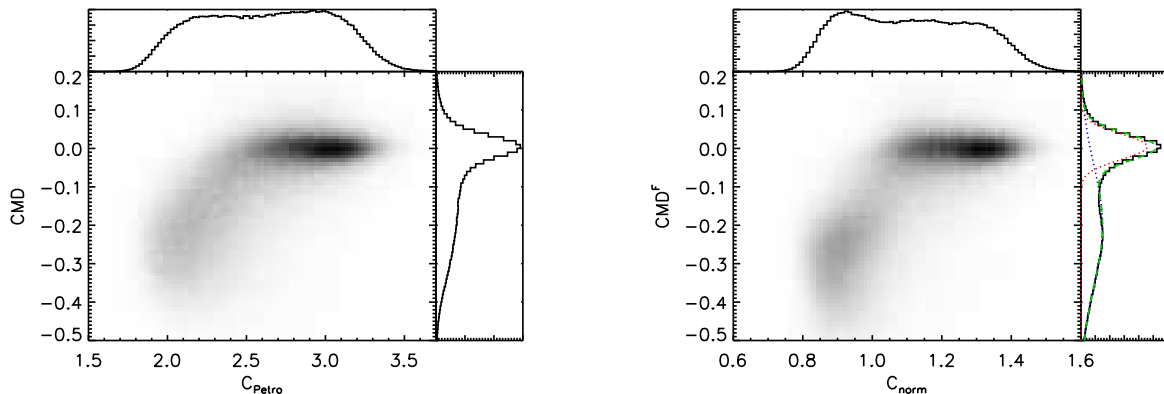


FIG. 2.— (*Left*) Distribution of Petrosian concentration  $C_{\text{Petro}}$  versus observed CMD location parameter for SDSS galaxies. The marginalized distributions are shown in the top histogram for  $C_{\text{Petro}}$  and the right histogram for CMD. (*Right*) As in the left panel for the inclination-corrected concentration  $C_{\text{norm}}$  and the face-on CMD location parameter  $\text{CMD}^F$ . The green dashed line in the  $\text{CMD}^F$  histogram shows the bimodal Gaussian fit to the distribution, while the red and blue dotted lines show the two components of the fit.

is much more bimodal than that of CMD: the previous blue tail that merged into the red sequence has become a distinct peak. We have employed the histogram fitting package RMIX (MacDonald 2007, see also our more extensive description in Paper I) to experiment with a range of possible multimodal fits that employ relatively simple basis functions (Gaussian, lognormal, gamma functions, etc.). Unlike the marginal distribution for  $C_{\text{norm}}$ , which clearly requires three components (see Paper I), a bimodal distribution fits the  $\text{CMD}^F$  histogram successfully with no clear evidence that would call for more than two components (see also Ellis et al. 2005). In Figure 2b, we show the best-fit RMIX solution that matches the  $\text{CMD}^F$  distribution as the sum of two Gaussian components. In this solution, 60% of the galaxies are assigned to the blue peak while 40% are assigned to the red peak. Finally, the separation between classes in the joint distribution is much stronger. Rather than simply lying in a spread-out tail, the late-type galaxies are relatively localized in a distinct and well-separated region of parameter space from the intermediate and early-type galaxies, which are themselves distinct.

In Figure 3 we have overplotted the locations of the visually classified galaxies onto the  $\text{CMD}-C_{\text{Petro}}$  and

$\text{CMD}^F-C_{\text{norm}}$  distributions. The symbol types and colors represent the visual classification. In both cases, the distribution at the low-concentration blue end is dominated by spiral galaxies while the high-concentration red end is dominated by elliptical galaxies. In the uncorrected distribution, the intermediate type galaxies span a wide range of parameter space, and in particular while elliptical galaxies dominate the high  $C_{\text{Petro}}$ -high CMD regime, there are also a large number of lenticular galaxies and a non-negligible number of spiral galaxies that also lie in this region of parameter space. In contrast, the separation between the regions is much cleaner in the inclination-corrected distribution. The inclination correction moves galaxies to the left and downward, almost completely evacuating the high  $C_{\text{norm}}$  region of spirals and spiral/lenticulars.

Based on the locations of visually classified galaxies on this plane and on the shape of the joint distribution, we have drawn a boundary in the  $C_{\text{norm}}-\text{CMD}^F$  plane to separate late-type galaxies from intermediate- and early-type galaxies, indicated by the solid line in the right panel of Figure 3. Within the intermediate- and early-type region of parameter space, there is some overlap in the distributions of the various visual classifications, although there is a clear trend for more later types

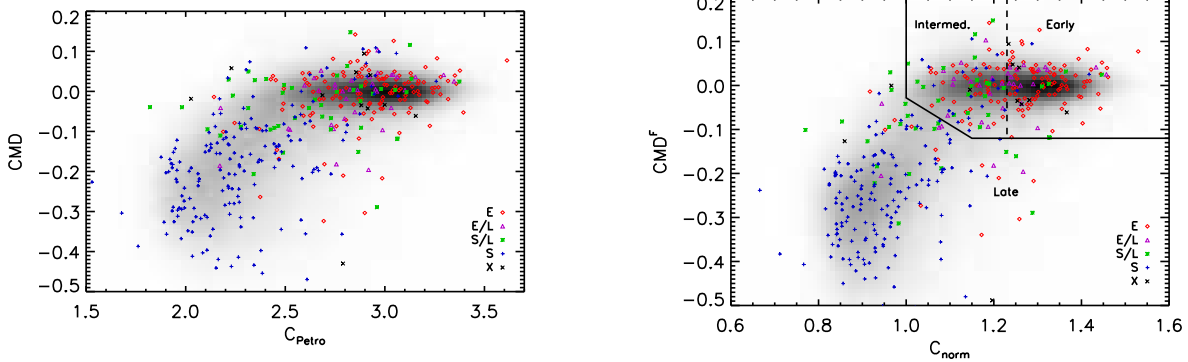


FIG. 3.— (Left) The grayscale denotes the distribution of Petrosian concentration parameters  $C_{\text{Petro}}$  versus observed CMD location parameter for SDSS galaxies, as in Figure 2. The locations of the visually classified galaxies are overlotted. The visual classifications are: elliptical (“E”, red diamonds), elliptical/lenticular (“E/L”, purple triangles), spiral/lenticular (“S/L”, green asterisks), spiral (“S”, blue pluses), and unclassifiable (“X”, black crosses). (Right) As in the left panel for the inclination-corrected concentration  $C_{\text{norm}}$  and the face-on CMD location parameter  $\text{CMD}^F$ . The solid line denotes our adopted boundary between late-type galaxies and intermediate/early-type galaxies, while the dashed line denotes a possible boundary between intermediate and early-type galaxies based on the trimodality of the  $C_{\text{norm}}$  parameter.

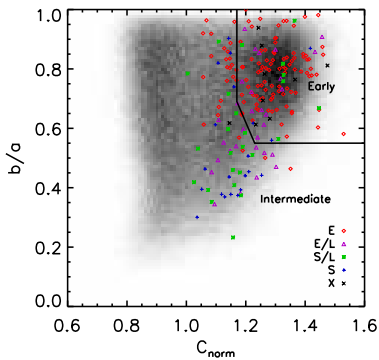


FIG. 4.— The grayscale denotes the distribution of inclination-corrected concentration  $C_{\text{norm}}$  versus isophotal  $b/a$  axis ratio for SDSS galaxies (see Paper I). The locations of visually classified galaxies that lie in the “Intermediate” and “Early” regions of Figure 3 are overlotted, with the same symbol types as in Figure 3. The solid line denotes our adopted separation between intermediate-type and early-type galaxies; this line is identical to the red line defining the boundary of early-type galaxies in figure 2 of Paper I.

at smaller  $C_{\text{norm}}$ . We tentatively place a border between intermediate- and early-type galaxies at  $C_{\text{norm}} = 1.23$  (indicated by the dashed line), which is the cross-over point between the intermediate and high- $C_{\text{norm}}$  peaks in the  $C_{\text{norm}}$  histogram (see Figure 2).

We have further examined the distribution of visually-classified galaxies in the axis ratio-concentration ( $b/a$ - $C_{\text{norm}}$ ) plane of Paper I. There are several reasons for doing this. Firstly, the overlap in the distribution of visually-classified galaxies of a given type within the Intermediate and Early regions of Figure 3 may perhaps be disentangled if the populations differ in another morphological parameter. Secondly, we note that in Paper I, we found that flattened galaxies with high  $C_{\text{norm}}$  have more in common with intermediate-concentration galaxies than with ellipticals. While this may suggest a problem with our inclination correction, the cause is simply statistics: the intrinsic axis ratio distribution of ellipticals drops off dramatically at low  $b/a$ , while the concentration distribution of intermediate-types is relatively

wide. Therefore, flattened galaxies with high  $C_{\text{norm}}$  are more likely to be unusually concentrated intermediate-types than unusually flattened ellipticals.

In Figure 4, we show the distribution of all SDSS galaxies as the grayscale, along with the visual classification of those galaxies that lie in the “Intermediate” and “Early” regions of Figure 3. The visual classification of these galaxies varies systematically as a function of axis ratio even at a constant concentration, and the ellipticals are very concentrated in the high- $C_{\text{norm}}$  high- $b/a$  region of parameter space. We therefore use this plane to separate early-type galaxies from intermediate-type galaxies as shown.

Our final classification is as follows:

- Early-type galaxies lie to the upper-right of the solid boundary in Figure 3 and to the upper-right of the boundary in Figure 4.
- Intermediate-type galaxies lie to the upper-right of the solid boundary in Figure 3 and to the bottom-left of the boundary in Figure 4.
- Late-type galaxies lie to the bottom-left of the solid boundary in Figure 3.

A comparison of our automated and visual classifications for each galaxy is given in Table 1. It can be seen that we do an excellent job of recovering the visual classification. 80% of our Early-type galaxies are classified by eye as E or E/L, while 90% of Late-type galaxies are classified as S or S/L by eye. This is as good as could be expected given that Ellis et al. (2005) found that two people independently visually classifying MGC images only agree at the  $\sim 80\%$  level.

The Intermediate classification, despite occupying a relatively limited region of parameter space, contains galaxies that have a range of visual morphologies. However, an examination of Figure 4 reveals that the visual classification of these galaxies, which have intrinsically very similar structural and photometric parameters, varies systematically with apparent axis ratio, i.e. inclination. While these galaxies contain disks, their passive

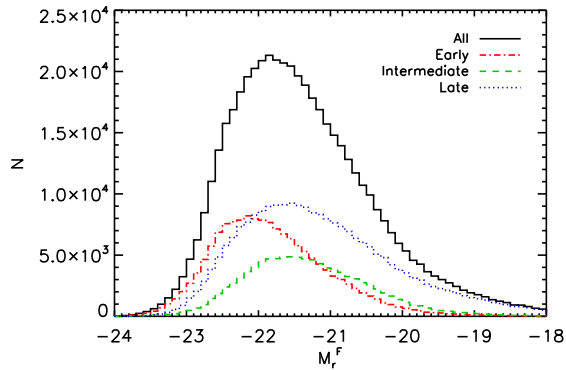


FIG. 5.— Face-on absolute magnitude distribution of all SDSS galaxies (black/solid), and those classified as Early (red/dot-dashed), Intermediate (green/dashed), and Late (blue/dotted).

appearance makes it difficult to identify the disk structure when seen face-on. Without the quantitative information available from the automated classification, it would be impossible to distinguish these galaxies from elliptical Early-type galaxies.

We evaluate the relative importance of each population as a function of luminosity by examining their absolute magnitude distribution (Figure 5). We recover the well-known result that the high-luminosity and low-luminosity ends of the galaxy population are dominated by early- and late-type galaxies respectively (e.g. Nakamura et al. 2003). As suggested in Paper I, the intermediate-type galaxies have a narrower luminosity distribution. Although a detailed analysis of the luminosity functions is beyond the scope of this paper, it is apparent from Figure 5 that the intermediate-type galaxies are unimportant at the faintest magnitudes, and therefore the observed intermediate types are representative of the population as a whole and not simply the tip of a large low-luminosity “iceberg”.

## 5. CONCLUSIONS

We have presented a new method to automatically classify galaxies from the SDSS or any equivalent survey given four basic photometric parameters: concentration, color, axis ratio, and absolute magnitude. This method explicitly corrects for inclination effects, allowing us to avoid the systematic misclassification of inclined versus face-on systems endemic to most other automated classifications. We prefer this method even over visual classification, usually considered to be the gold standard, which has considerable person-to-person scatter (see Ellis et al. 2005) and is also susceptible to systematic inclination biases, as suggested by the variation of visual classifications as a function of axis ratio along the intermediate  $C_{\text{norm}}$  locus in Figure 4.

In Paper I, we discovered that applying an inclination correction to the observed concentration of SDSS galaxies tightens an apparently bimodal distribution into three distinct peaks. In this work, we have discovered that correcting colors and absolute magnitudes for inclination effects also tightens the “blue cloud” of the CMD into a much more distinct peak in parameter space (see also Unterborn & Ryden 2008). Based on the joint distribution of concentration and CMD location, we find that the galaxy population separates well into *three* distinct classes, labeled here as “Early”, “Intermediate”, and “Late”. We have validated our classification scheme

by comparing to visual classifications of a subset of galaxies in the high-quality MGC images.

A consequence of the results presented here and in Paper I is that there is an Intermediate galaxy type, distinct from both Early-types (traditional ellipticals) and Late-types (traditional spirals). These galaxies have intermediate concentrations consistent with typical bulge-to-disk ratios of  $\sim 3$ , a wide range of apparent axis ratios implying a disk morphology, and colors indistinguishable from those of ellipticals of the same luminosity (i.e. the CMD<sup>F</sup> distributions are similar, although this corresponds to a bluer median color for the Intermediate types due to their lower median luminosity). Intermediate types span the full range of visual classifications, although this may be more indicative of the fallibility of visual classification than of the intrinsic properties of Intermediate types.

It is interesting to contrast our galaxy types to those of Weinmann et al. (2006), who also identified an intermediate class of galaxy. However, their intermediate types do not clump in one particular region of parameter space but rather lie at the intersection of the early- and late-type populations. These authors consider that their intermediate-types may be (a) edge-on reddened late-type galaxies, (b) early-type galaxies whose star formation rates are overestimated, (c) a mixture of (a) and (b) (their preferred explanation), or (d) a distinct population. Our intermediate-types cannot be (a), because we have explicitly corrected for inclination, nor (b) or (c), because the star formation rate does not enter into our classification. Therefore, unlike the intermediate-types identified by Weinmann et al. (2006), our Intermediate classification must represent a truly distinct galactic population. The lenticulars and bulgy disks that constitute our Intermediate type are red and passive, and would be classified as “early” in Weinmann et al. (2006).

The standard explanation for the bimodality of the CMD is that galaxies remain blue and star-forming while they contain cold gas, but at some point in their evolution they rapidly lose their cold gas (perhaps due to ram pressure stripping, strangulation, or galaxy harassment when entering a dense cluster or group environment; removal of gas through a galactic wind or active galactic nucleus; or exhaustion of their fuel in a merger-induced starburst), and quickly transit to the red sequence as the young stars fade. Our discovery that there are two distinct populations on the red sequence, an intermediate-concentration population that contains a disk and a high-concentration population that is entirely spheroidal, suggests that there are two distinct mechanisms for transiting to the red sequence. We propose that Intermediate-type galaxies are those whose gas-removal process did not significantly perturb the global morphology of the galaxy (e.g. strangulation), while Early-type galaxies are those whose gas was removed in a violent event like a major merger. Alternatively, perhaps there is only one method of transiting to the red sequence, which results in Intermediate-type galaxies, while Early-types are formed from violent “dry” mergers of Intermediate and Early-type galaxies. Regardless, the presence of these distinct populations provides a key observational clue to the processes that drive galaxy evolution.

It is important to note that our samples consist of galaxies within the local universe, i.e. which have had

a Hubble time for their structure to regularize. Classification methods based on local galaxies might not apply to younger high redshift galaxies. Determining the epoch when these regular patterns emerged would provide an important constraint in their origin.

JB thanks Joe Liske for help with the MGC database and the SDSS help desk for their help with the Catalog Archive Server.

Funding for the Sloan Digital Sky Survey (SDSS) and SDSS-II has been provided by the Alfred P. Sloan Foundation, the Participating Institutions, the National Science Foundation, the U.S. Department of Energy, the National Aeronautics and Space Administration, the Japanese Monbukagakusho, and the Max Planck Society, and the Higher Education Funding Council for England. The SDSS Web site is <http://www.sdss.org/>.

The SDSS is managed by the Astrophysical Research Consortium (ARC) for the Participating Institutions. The Participating Institutions are the American Museum of Natural History, Astrophysical Institute Potsdam, University of Basel, University of Cambridge, Case Western Reserve University, The University of Chicago, Drexel University, Fermilab, the Institute for Advanced

Study, the Japan Participation Group, The Johns Hopkins University, the Joint Institute for Nuclear Astrophysics, the Kavli Institute for Particle Astrophysics and Cosmology, the Korean Scientist Group, the Chinese Academy of Sciences (LAMOST), Los Alamos National Laboratory, the Max-Planck-Institute for Astronomy (MPIA), the Max-Planck-Institute for Astrophysics (MPA), New Mexico State University, Ohio State University, University of Pittsburgh, University of Portsmouth, Princeton University, the United States Naval Observatory, and the University of Washington.

The Millennium Galaxy Catalogue consists of imaging data from the Isaac Newton Telescope and spectroscopic data from the Anglo Australian Telescope, the ANU 2.3m, the ESO New Technology Telescope, the Telescopio Nazionale Galileo and the Gemini North Telescope. The survey has been supported through grants from the Particle Physics and Astronomy Research Council (UK) and the Australian Research Council (AUS). The data and data products are publicly available from <http://www.eso.org/~jliske/mgc/> or on request from J. Liske or S.P. Driver.

*Facilities:* Sloan, ING:Newton, AAT, ATT, NTT, TNG, Gemini:Gillett

## REFERENCES

- Adelman-McCarthy, J. K., et al. 2007, ApJS, submitted, arXiv:0707.3413
- Bailin, J., & Harris, W. E. 2008, MNRAS, in press, arXiv:0801.2774 (Paper I)
- Baldry, I. K., Glazebrook, K., Brinkmann, J., Ivezić, Ž., Lupton, R. H., Nichol, R. C., & Szalay, A. S. 2004, ApJ, 600, 681
- Balogh, M. L., Baldry, I. K., Nichol, R., Miller, C., Bower, R., & Glazebrook, K. 2004, ApJ, 615, L101
- Blanton, M. R., et al. 2003a, AJ, 125, 2348
- Blanton, M. R., et al. 2003b, ApJ, 594, 186
- de Vaucouleurs, G. 1948, Annales d'Astrophysique, 11, 247
- Driver, S. P., et al. 2006, MNRAS, 368, 414
- Driver, S. P., Popescu, C. C., Tuffs, R. J., Liske, J., Graham, A. W., Allen, P. D., & de Propris, R. 2007, MNRAS, 379, 1022
- Ellis, S. C., Driver, S. P., Allen, P. D., Liske, J., Bland-Hawthorn, J., & De Propris, R. 2005, MNRAS, 363, 1257
- Hubble, E. P. 1926, ApJ, 64, 321
- Liske, J., Lemon, D. J., Driver, S. P., Cross, N. J. G., & Couch, W. J. 2003, MNRAS, 344, 307
- MacDonald, P. D. M. 2007, documentation and code at <http://www.math.mcmaster.ca/peter/mix/mix.html>, Department of Mathematics and Statistics, McMaster University
- Maller, A. H., Berlind, A. A., Blanton, M. R., & Hogg, D. W. 2008, ApJ, submitted, arXiv:0801.3286
- Nakamura, O., Fukugita, M., Yasuda, N., Loveday, J., Brinkmann, J., Schneider, D. P., Shimasaku, K., & SubbaRao, M. 2003, AJ, 125, 1682
- Sérsic, J. L. 1968, Atlas de galaxias australes (Cordoba, Argentina: Observatorio Astronomico, 1968)
- Shao, Z., Xiao, Q., Shen, S., Mo, H. J., Xia, X., & Deng, Z. 2007, ApJ, 659, 1159 (S07)
- Strateva, I., et al. 2001, AJ, 122, 1861
- Strauss, M. A., et al. 2002, AJ, 124, 1810
- Unterborn, C. T., & Ryden, B. S. 2008, ApJ, submitted, arXiv:0801.2400
- Weinmann, S. M., van den Bosch, F. C., Yang, X., & Mo, H. J. 2006, MNRAS, 366, 2
- Yamauchi, C., et al. 2005, AJ, 130, 1545
- York, D. G., et al. 2000, AJ, 120, 1579